Ocean Sci. Discuss., 7, 1703–1737, 2010
www.ocean-sci-discuss.net/7/1703/2010/
doi:10.5194/osd-7-1703-2010

Ocean Science Discussions

A new assimilation tidal model for the Mediterranean Sea

D. N. Arabelos, D. Z. Papazachariou, M. E. Contadakis, and S. D. Spatalas

Department of Geodesy and Surveying, Aristotle University of Thessaloniki, 54124 Thessaloniki, Greece

Received: 7 September 2010 – Accepted: 15 September 2010 – Published: 30 September 2010

Correspondence to: D. N. Arabelos (arab@eng.auth.gr)

Published by Copernicus Publications on behalf of the European Geosciences Union.

Abstract

The tides for the Mediterranean Sea are described through a high resolution model (MEDI10) developed by assimilation of data into the global TPXO7.2 ocean tide model. Tidal parameters from 54 coastal tide-gauge stations around Mediterranean for eight principal constituents: M2, S2, N2, K2, K1, O1, P1 and Q1 and from 20 stations for M2, S2, K1, O1 are included in the model. TOPEX/Poseidon data with all corrections applied except for the ocean tides and bathymetry from ETOPO2 were used for development of the model. The tidal parameters used in the assimilation procedure were compared with corresponding parameters extracted from the model. Comparisons were carried out with other published global or regional models. Furthermore, an assessment was resulted comparing crossover differences from JASON-1 altimetry corrected for ocean tides using MEDI10 and other published global or regional models.

1 Introduction

Ocean tides especially in closed sea areas can deviate considerably from the theoretical values due to unequal water depths and to the fact that the continents impede the movement of water. Satellite altimetry enabled the development of improved tidal models even in closed sea areas, by assimilating altimeter data into hydrodynamic models. In general, the modern global tidal models can be categorized into three groups: hydrodynamic, empirical, and assimilation models.

Hydrodynamic models are derived by solving the Laplace Tidal Equations (LTE) and using bathymetry data as boundary conditions. Most of hydrodynamic solutions, such as Schwiderski's (1980) and FES94.1 (Le Provost et al., 1994) are undefined in the Mediterranean Sea, due to its bottom morphology and coast complexity (see Fig. 1).

Empirical models are derived by extracting ocean tidal signals from satellite altimetry and they describe the total geocentric ocean tides, which include the ocean loading effect. These models can be used directly in altimetry applications such as ocean tide corrections.

OSD

7, 1703–1737, 2010

Assimilation models are derived by solving the hydrodynamic equations with altimetric and tide-gauge data assimilation. The tides are constrained by the hydrodynamic equations which must satisfy the tidal fields of elevations and velocities, and the observation data from tide-gauge stations and altimetry. Generalized inverse methods allow the combination in a rational manner all of this information into tidal fields best fitting both the data and the dynamics, in a least squares sense (Bennett, 1992; Egbert et al., 1994).

Basins such as the Mediterranean Sea, which are connected to the oceans through narrow entrances, have small tidal ranges (Pugh, 1987). The areas of entrances are too small for sufficient oceanic tidal energy to enter to compensate for the energy losses which would be associated with large tidal amplitudes. This is the main reason of the weakness of the Mediterranean tides. Although the amplitude of the tides in the Mediterranean Sea is small, the use of the best current tidal model is very essential for many geodetic and geodynamic applications (e.g., Arabelos, 2002).

The Mediterranean Sea is divided into two large basins separated by the Sicilian Channel and the Straits of Messina. The tides of the western basin are strongly influenced by the Atlantic tides which penetrate through the Straits of Gibraltar. Apart from the strait of Gibraltar, two smaller openings of the Mediterranean to the Bosporus (N-E Aegean) and the Suez (S-E Mediterranean) channels are negligible for tidal propagation studies. The Adriatic and Aegean Seas are connected to the eastern basin through the Straits of Otranto and Crete, respectively. The configuration of the eastern basin is very complicated. The bathymetry of the Mediterranean Sea is quite complex with both the east and west basins being more than 4 km deep in places (see Fig. 1).

Problems in tidal studies are due to the inadequate number of tide-gauge stations mainly along the south and east coasts of the Mediterranean and in the quality of the existing data. The lack of data from deep areas is balanced by the good quality altimeter data gained e.g. from TOPEX/Poseidon and JASON-1. Existed global and regional models such as GOT00.2 (Ray, 1999), NAO99.b (Matsumoto et al., 2000), TPXO7.2 (Egbert et al., 1994), MED2008 (Egbert and Erofeeva, 2008), succeed in describing

OSD
7, 1703–1737, 2010

satisfactory the tidal propagation in the main part of the basin, thought the use of an adequate number of coastal data might improve further the up to now achieved quality.

Here we present a new numerical model for the Mediterranean Sea hereinafter referred to as MEDI10. The assimilation method selected for the computation is described in brief in Sect. 2. In Sect. 3 the data used for the computation and the assessment of the model are described. Details about the tide-gauge observations, their method of analysis and the corresponding results are given in Sect. 4. In Sect. 5 the computed model is described. The assessment of the model, using various methods is described in Sect. 6. Conclusions and remarks are drawn in Sect. 7.

2 Method

For the computation of the tidal model the "Oregon State University Tidal Inversion Software" (OTIS) was used (Egbert and Erofeeva, 2002). The OTIS assimilation method determines the optimal tidal solution that satisfies the tidal dynamics and simultaneously provides the best overall fit to the assimilation observations. More explicitly the goal of the method is to find tidal fields $\boldsymbol{u}$ consisted both with the hydrodynamic equations

$$\mathbf{S}\boldsymbol{u} = \boldsymbol{f}_0, \tag{1}$$

where $\mathbf{S}$ is the dynamical equations plus boundary conditions and $\boldsymbol{f}_0$ is the astronomical forcing corrected for solid Earth tides, and with a k-dimensional vector $\boldsymbol{d}$ of tidal data

$$\boldsymbol{d} = \mathbf{L}\boldsymbol{u}. \tag{2}$$

In Eq. (2) $\mathbf{L}$=[$L_1 \ldots L_k$] corresponds to the k measurement functionals relating variables from data space to the unknown tidal space $\boldsymbol{u}$. Due to measurement errors and inadequacies in the necessarily approximate dynamical equations, there will be in general no $\boldsymbol{u}$ satisfying both equations. With the generalized inversion approach

OSD
7, 1703–1737, 2010
A new assimilation tidal model for the Mediterranean Sea
D. N. Arabelos et al.

a compromise between Eqs. (1) and (2) is achieved by minimizing the quadratic penalty functional

$$J[\boldsymbol{d},\boldsymbol{u}] = (\mathbf{L}\boldsymbol{u}-\boldsymbol{d})^{\mathrm{T}}\boldsymbol{\Sigma}_{\mathbf{e}}^{-1}(\mathbf{L}\boldsymbol{u}-\boldsymbol{d}) + (\mathbf{S}\boldsymbol{u}-\boldsymbol{f}_0)^{\mathrm{T}}\boldsymbol{\Sigma}_{\mathbf{f}}^{-1}(\mathbf{S}\boldsymbol{u}-\boldsymbol{f}_0), \tag{3}$$

where $\boldsymbol{\Sigma}_{\mathbf{e}}$ is the measurement error covariance and $\boldsymbol{\Sigma}_{\mathbf{f}}$ is the model covariance error. The penalty function Eq. (3) consists of two main terms, the error to the data and the error to the model and the aim is to determine the optimal space $\boldsymbol{u}$ that minimize the penalty function J. If the dynamical equations (Eq. 1) are linear, the reduced basis representer method (Bennett, 1992), can be used to minimize (Eq. 3) according to which representers, i.e. functions showing the impact that a single observation will have on the entire domain, are calculated for a subset of data locations and a solution to the variational problem is sought within the space of linear combinations of calculated representers. The minimizer of Eq. (3) can be written as

$$\hat{\boldsymbol{u}} = \boldsymbol{u}_0 + \sum_{k=1}^{K} \beta_k \boldsymbol{r}_k, \tag{4}$$

where $\boldsymbol{u}_0 = \mathbf{S}^{-1}\boldsymbol{f}_0$ is the exact solution of Eq. (1), the functions $\boldsymbol{r}_k$ are the representers of the data functionals defined by L_k and $\beta_k, (k=1,K)$ are coefficients to be determined.

Representers can be calculated by first solving the adjoint of the dynamical equation

$$\mathbf{S}^{\mathrm{T}} a_k = \Delta_k, \tag{5}$$

where Δ_k is the averaging kernel for the data functional L_k, and then solving the forward equation

$$\mathbf{S}\boldsymbol{r}_k = \boldsymbol{\Sigma}_{\mathbf{f}}\, a_k. \tag{6}$$

The forcing for Eq. (6) is the solution to Eq. (5) smoothed by convolution with the dynamical error covariance $\boldsymbol{\Sigma}_{\mathbf{f}}$.

The representer coefficients β_k are found by solving the $K \times K$ system of equations

$$(\mathbf{R}+\boldsymbol{\Sigma}_{\mathbf{e}})\,\beta = \boldsymbol{d} - \mathbf{L}\boldsymbol{u}_0, \tag{7}$$

OSD
7, 1703–1737, 2010
A new assimilation tidal model for the Mediterranean Sea
D. N. Arabelos et al.

where $\mathbf{R}$ is the representer matrix with elements

$$R_{jk} = \mathbf{L}_j \boldsymbol{r}_k. \tag{8}$$

To describe the dynamics of the tides, the linearized shallow water equations are used

$$\frac{\partial \boldsymbol{U}}{\partial t} + f\hat{\boldsymbol{z}} \times \boldsymbol{U} + gH\nabla(\zeta - \zeta_{\mathrm{SAL}}) + \boldsymbol{F} = \boldsymbol{f}_0,$$

$$\frac{\partial \zeta}{\partial t} = -\nabla \cdot \boldsymbol{U}, \qquad \boldsymbol{U} = \begin{bmatrix} U \\ V \end{bmatrix}, \tag{9}$$

where U and V are the two components of the barotropic transport i.e., the depth-averaged velocity times the depth H, f is the Coriolis parameter, $\hat{\boldsymbol{z}}$ is oriented to the local vertical, t is the time, $\boldsymbol{F}$ is the dissipative stress, g is the acceleration of gravity, ζ is the elevation of the sea surface, ζ_{SAL} is the tidal loading and self attraction and $\boldsymbol{f}_0$ represents the earth tide.

The linearized OTIS dynamics can be transformed from the time domain into the frequency domain using Fourier transform. In this way the Eq. (9) can be expressed by the following time-independent equations

$$\boldsymbol{\Omega U} + gH\nabla\zeta = \boldsymbol{f}_U, \tag{10}$$

$$\nabla \cdot \boldsymbol{U} + i\varpi\zeta = \boldsymbol{f}_\zeta, \tag{11}$$

where

$$\boldsymbol{\Omega} = \begin{bmatrix} i\varpi + k & -f \\ f & i\varpi + k \end{bmatrix}.$$

Assuming $k \neq 0$ or $\varpi \neq f$, $\boldsymbol{\Omega}$ is invertible at all locations, so that Eq. (10) can be written as

$$\boldsymbol{U} = -gH\boldsymbol{\Omega}^{-1}\nabla\zeta + \boldsymbol{\Omega}^{-1}\boldsymbol{f}_U \tag{12}$$

OSD
7, 1703–1737, 2010

and combine this with Eq. (11) a second order equation in ζ is gained

$$\nabla \cdot gH\boldsymbol{\Omega}^{-1}\nabla\zeta - i\omega\zeta = \nabla\cdot\boldsymbol{\Omega}^{-1}\boldsymbol{f}_U + \boldsymbol{f}_\zeta. \tag{13}$$

Solution of Eq. (1) can thus be accomplished by solving Eq. (13) for ζ, then using the result in Eq. (12) to calculate $\boldsymbol{U}$. This provides in brief the basic scheme for solving shallow water equations. The method and its numerical implementation are described in details by Egbert et al. (1994); Egbert and Erofeeva (2002).

3 Data

The following data sets were used in this investigation:

- PATHFINDER data base including TOPEX/Poseidon altimeter data for the period 23 September–11 August 2002, with no-tidal correction applied.
- ETOPO2 bathymetry model.
- Tide-gauge data: Hourly values from 59 tide-gauge stations in the Mediterranean Sea (see Fig. 2) were analyzed. In Table 1 details about the time coverage of the data are shown.
- Tidal parameters for M2, S2, K1, O1 from 20 tide-gauge stations extracted from Tsimplis et al. (1995) (see Fig. 2).
- TPXO7.2 global tidal model.
- JASON-1 altimeter data for the period 15 January 2002–16 May 2004, as an independent source of assessment.

TPXO7.2 is a current version of a global model of ocean tides, which best-fits, in a least-squares sense, the Laplace Tidal Equations and along track averaged data from TOPEX/Poseidon and JASON-1, obtained with OTIS.

We have not used the new pathfinder altimetry data base including JASON-1 data (personal communication, Beckley, 2010), because JASON-1 data are used to assess our model. More specifically, we examine the statistics of the crossover differences of JASON-1 altimetry before and after tidal corrections using MEDI10 as well as other recent tidal models.

4 Analysis of the tide-gauge observations

Data from 59 tide-gauge stations distributed mostly along the north coasts of the Mediterranean Sea (see Fig. 2, red dots) were available from different organizations as it is shown in Table 1. These data were hourly values covering time periods from one to almost fifteen years as it is indicated in Table 1. The analysis of the coastal data was carried out using the "Versatile Harmonic Tidal Analysis" software (Foreman et al., 2009). This software permits more versatility in the harmonic analysis of tidal time series.

Specific improvements to traditional methods include the analysis of randomly sampled and/or multiyear data, more accurate nodal correction, inference and astronomical argument adjustments through direct incorporation into the least squares matrix and correlation matrices and error estimates, using Singular Value Decomposition (SVD) techniques. This approach facilitate decisions on the selection of constituents for the analysis. In mathematical terms, a one-dimensional time series with tidal and no-tidal energies can be expressed by

$$h(t_j) = Z_0 + \sum_{k=1}^{n} f_k(t_0) A_k \cos[\omega_k(t_j - t_0) + V_k(t_0) + u_k(t_0) - g_k] + R(t_j), \tag{14}$$

where $h(t_j)$ is the measurement at time t_j, Z_0 is a constant, $f_k(t_0)$ and $u_k(t_0)$ are the nodal corrections to amplitude and phase, respectively, at some reference time t_0, for major constituent k with frequency ω_k, A_k, and $g_k (k = 1,n)$ are the amplitude and phase lag of constituent k, respectively, $V_k(t_0)$ is the astronomical argument for constituent k at time t_0, $R(t_j)$ is the no-tidal residual, and n is the number of tidal constituents. To solve for Z_0, A_k and g_k, a least squares approach is usually used. The observation times are assumed to arise from hourly sample with gaps permitted. In order to avoid some deficiencies and limitations, the basic Eq. (14) was replaced by

$$h(t_j) = Z_0 + a\,t_j + \sum_{k=1}^{n} f_k(t_j)A_k\cos[V_k(t_j) + u_k(t_j) - g_k] + R(t_j), \tag{15}$$

where a is a linear trend. According to Foreman et al. (2009), the advantage in this case is that V, $\boldsymbol{u}$ and $\boldsymbol{f}$ are evaluated at the precise times of each measurement, thus eliminating inaccuracies arising from the assumption of a linear variation in the astronomical argument and temporally constant values for the nodal corrections. Furthermore, the linear trend allows for the measurements t_j to arise from arbitrary sampling, and permits multi-constituent inferences that are computed directly within the least squares fit.

In the harmonic analysis 15 tidal constituents are included (Z_0, MM, MF, Q1, O1, K1, MU2, N2, M2, S2, MK3, SK3, S4, 2SM6, M8). Constituents P1 and K2 are inferred from K1 and S2, respectively, using the exact amplitude ratios and phase differences used in the synthesis. The rms residual error for the 59 tide-gauge stations ranges from 8 to 10 cm depending on the length and the quality of each tidal time series. The SVD approach produces a covariance matrix and correlation coefficients

$$r_{jk} = \mathrm{cov}(x_j, x_k)/[\sigma(x_j)\sigma(x_k)] \tag{16}$$

that allow a direct method for evaluating the independence of the chosen constituents (Cherniawsky et al., 2001). In Table 2 correlation coefficients larger than 0.01 related to the corresponding station (number in parenthesis) between the constituents j and k of the corresponding covariance matrices are shown. Maximum values are shown between MU2 and N2 (equal to 0.068) and between Z_0 and MM (equal to 0.052). Taking into account these results, 8 major constituents (M2, S2, K1, O1, N2, P1, K2 and Q1) were used for the computation of the model. For the southern coasts of the

Mediterranean Sea where no tide-gauge data were available the tidal parameters M2, S2, O1, K1 from Tsimplis et al. (1995) were used at 20 stations (Fig. 2, blue dots).

5 Computation of the model

The model grid is $2' \times 2'$, which correspond to about 3.7 km in latitude and 2.9 km in longitude (for mean latitude equal to 37.5). The model was computed using the FORTRAN 90 package of OTIS. The following parameters were used:

- Constant friction velocity equal to 2 m/s
- Decorrelation length scale equal to 37 km
- Decorrelation length scale for Open Boundaries equal to 370 km
- Fractional bathymetry error 0.05
- Fractional drag error 0.55
- Length scale for variance 37 km
- Fractional open boundary error 0.05
- Fractional rigid boundary error 0.2

The number of open boundaries was equal to 144. The number of representers was 271 (197 from altimetry and 74 from coastal stations).

The data of the stations 3, 13, 31, 45 and 53 (see Fig. 2) were excluded from the computations because a) of their vicinity to other stations and b) their amplitudes and phases differ considerably. For instance, the amplitudes of the stations very close to the strait of Gibraltar (numbers 3, 13, 20 and 53 in Fig. 2) range from 29.9 to 41.3 cm and their phases from 40.99 to 49.6 degrees. As a criterion for the rejection was the comparison of the quality of the data, based on the standard deviation of the analysis

OSD
7, 1703–1737, 2010

results. In Fig. 3 the distribution of the representers (red) and data sites (yellow) are shown.

Figure 4 shows the computed amplitude and phase of the M2 tide. The amplitude in the most part of the basin is less than 10 cm, with the exception of the Gulf of Gabes (53 cm), the North Adriatic (22 cm) and the strait of Gibraltar (40 cm). Two amphidromes are clearly defined: the first one in the strait of Sicily and the second in the North Adriatic. The degenerate amphidrome between the north coast of Africa and Crete is in agreement with other numerical models. The amphidrome in western basin appeared in other numerical models (e.g., Tsimplis et al., 1995) is more clearly described in Fig. 5, showing the amplitude and phase of S2 tide. In this Fig. the amplitude pattern is very similar to those of M2 but with reduced amplitudes.

Figure 6 shows the computed amplitude and phase of the major diurnal K1 tide. It is noteworthy the large amplitude of 16 cm existing only in the Adriatic Sea. There is only one amphidrome evident at the strait of Sicily. The amplitude and phase of the diurnal O1 constituent are shown in Fig. 7.

Figures 8–11 show the computed amplitude and phase of the W-E and S-N transports for M2 constituent. The amplitudes of the W-E transport are in most parts of the basin of the order of one to several $m^2 s^{-1}$, with increasing values south of Crete, in the straits of Sicily, the Alboran Sea and with a maximum reaching 306 $m^2 s^{-1}$ in the straits of Gibraltar.

The amplitude of the S-N transports of M2 constituent shows two characteristic patterns with amplification zones in the eastern and western basins of the Mediterranean Sea. In the eastern basin the amplification zones are directed from S-E to N-W, along the Aegean Sea, the Adriatic channel, reaching a maximum of 16 $m^2 s^{-1}$ at the strait of Sicily. In the western basin the direction is changing from S-W to N-E and the amplitude takes its maximum of 100 $m^2 s^{-1}$ in the straits of Gibraltar.

6 Assessment

The differences d between the modeled a_m and g_m and observed a_0 and g_0 harmonic constants are calculated as vectorial differences using the formula (Foreman et al., 1993)

$$d = \left[(a_0 \cos g_0 - a_m \cos g_m)^2 + (a_0 \sin g_0 - a_m \sin g_m)^2\right]^{1/2}. \tag{17}$$

The results of the comparison between the 54 observed harmonic constants used in our solution and the harmonic constants extracted from our model are shown in Table 3. In Table 5 corresponding results are shown from the comparison between the harmonic constants from Tsimplis et al. (1995) used also in our solution and the harmonic constants from our model.

More specifically, in Table 3 vectorial differences according to Eq. (17) between all modeled and observed constituents are shown. For M2 differences of the order of cm or below are shown in most sites, though larger differences ranging between 2 and 7 cm are shown in the North Adriatic (Split, Trieste, Venezia, Zadar), in the North Aegean (Thessaloniki, Alexandroupolis) as well as in Toulon, Porto Torres, Messina, Civitavecchia, Mellila and Antalya. Significant differences are shown in the North Adriatic also for S2, K1, O1, and P1. The statistics of the differences at all sites of each tidal constituents of Table 3 is shown in Table 4.

Significant vectorial differences between modeled and harmonic constants from Tsimplis et al. (1995) are shown in Table 5 for M2 and S2 in the Gulf of Gabes and Sfax.

The statistics of the differences at all sites of each tidal constituents of Table 5 is shown in Table 6.

A possibility to have an external assessment of tidal models comes through the comparison of the results of tidal correction applied on heterogeneous data such as the altimeter data. However, altimeter data from T/P and ERS1/2 are correlated to recent models since they have been used for the development of them. For this reason,

OSD
7, 1703–1737, 2010

JASON-1 data have been used instead of T/P and ERS1/2. For this purpose altimeter data from JASON-1 GDRs (AVISO & PODAAC, 2001) were extracted from cycles 1 to 86 with the exception of cycle 69, covering the Mediterranean Sea. The data were corrected due to ionospheric, wet and dry tropospheric effect, sea state bias, inverse barometric effect and solid earth tide. We avoided performing ocean tide correction using the tidal models provided on the JASON-1 GDR in order to assess the tidal models under consideration. Flagged data with radiometer surface type 1 (land) were removed. In order to eliminate outliers the remaining data were reduced to EGM96 geopotential model, and SSH with absolute difference JASON-EGM96>2 m were considered as outliers and therefore were eliminated. The assessment was based on the comparison of the statistics of the crossover differences of JASON-1 SSH, before and after tidal correction, using MEDI10 and the models MED2004 (an earlier Mediterranean inverse tidal solution by Egbert and Erofeeva), MED2008, GOT00.2 and NAO99b. The results of this experiment in terms of the statistics of the crossover differences before and after the geocentric tidal correction are shown in Table 7.

The best improvement in terms of the standard deviation of the crossover differences is resulted after the tidal correction using MED2008 and MEDI10. Both models are computed with the same method. The differences between them are the following: MEDI10 is using the 2 min bathymetry model ETOPO2, 3688 data sites of TOPEX/Poseidon altimetry and the tide-gauge data described in Sect. 4. MED2008 is using the GEBCO 1 min bathymetry, more than 9000 data sites of 531 cycles of TOPEX and JASON-1 and 114 cycles of JASON-2. It means that MED2008 is somehow correlated with JASON-1.

The comparison of our model with other models can also be expressed in another way, namely by computing the statistics of the discrepancies of tidal heights from the models under consideration at different time moments. For this reason, tidal heights were computed from the models MEDI10, MED2008, GOT00.2 and NAO99b on a $15' \times 15'$ grid at a number of different time moments selected randomly within the time period between August 2007 and May 2011. It was found that 20 such grids were sufficient to give a stable estimate in terms of standard deviation for the three pairs of the models. The statistics of this comparison is shown in Table 8. The number of differences for each pair (column 2) varies, depending on the common points of the grid where the computation of tidal height was possible from both models of the pair. Table 8 shows that the best agreement in terms of standard deviation occurred between MED2008 and MEDI10.

7 Summary and conclusions

A regional model for the Mediterranean Sea was computed using bathymetry, altimeter data and data from coastal tide-gauge stations. The method used for the computation of the model was the inverse modeling of barotropic ocean tides. Tide-gauge data were selected from different national or international organizations. The analysis of these observations was carried out using the "Versatile Harmonic Tidal Analysis" method. The problems in this study were caused by the lack of adequate number of tide-gauges around the east and south part of the Mediterranean coasts and by discrepancies between the tidal parameters of neighboring stations. The quality of the computed model was estimated by internal and external assessment. The comparison with other recent models shows generally an agreement ranging between 1 and 2 cm in terms of the standard deviation of the computed tidal heights. The comparison of the standard deviation of the crossover differences of JASON-1 before and after tidal correction using MEDI10 and other models shows also comparable results. The impact of parameters used, such as the friction velocity, the decorrelation length scale for open boundaries, the hypotheses for fractional bathymetry and fractional open boundary errors, have to be numerically investigated in future experiments, with simultaneous use of more recent data.

Acknowledgements. We are very grateful to Svetlana Erofeeva for her continuous support in all phases of this (first for us) experiment and for providing an improved version of OTIS package. Many thanks are due to Mike Foreman and Josef Cherniawsky for providing their tidal analysis packages and Guy Woppelmann for providing French tide-gauge data.

References

Arabelos, D.: Comparison of Earth-tide parameters over a large latitude difference, Geophys. J. Int., 151, 950–956, 2002. 1705

AVISO and PODAAC User Handbook: IGDR and GDR Jason Products, Toulouse, 2001. 1715

Bennett, A. F.: Inverse Methods in Physical Oceanography. Monographs on Mechanics and Applied Mathematics, Cambridge University Press, Cambridge, 346 pp., 1992. 1705, 1707

Cherniawsky, J. Y., Foreman, M. G. G., Crawford, W. R., and Henry, F. R.: Ocean tides from TOPEX/Poseidon sea level data, J. Atmos. Ocean. Tech., 18, 649–664, 2001. 1711

Egbert, G., Bennett, A., and Foreman, M. G. G.: TOPEX/Poseidon tides estimated using a global inverse model, J. Geophys. Res., 99, C12, 24821–24852, 1994. 1705, 1709

Egbert, G. and Erofeeva, S.: Efficient inverse modelling of barotropic ocean tides, J. Atmos. Ocean. Tech., 19(2), 183–204, 2002. 1706, 1709

Egbert, G. and Erofeeva, S.: Mediterranean inverse tidal solution, available at http://volkov.oce.orst.edu/tides/region.html, 2008. 1705

Foreman, M. G. G.: Manual for tidal heights analysis and prediction, Pacific Marine Science, Rep. 77-10, Institute of Ocean Sciences, Patricia Bay, Sidney, BC, 66 pp., 1977.

Foreman, M. G. G.: The harmonic analysis of tidal model time series, Adv. Water Resour., 12, 109–120, 1989.

Foreman, M. G. G., Henry, R. F., Walters, R. A., and Ballantyne, V. A.: A finite element model for tides and resonance along north coast of British Columbia, J. Geophys. Res., 98, 2509–2531, 1993. 1714

Foreman, M. G. G., Cherniawsky, J. Y., and Ballantyne, V. A.: Versatile harmonic tidal analysis: improvements and applications, J. Atmos. Ocean. Tech., 26(4), 806–817, 2009. 1710, 1711

Le Provost, C., Genco, M. L., Lyard, P., Vincent, P., and Canceil, P.: Tidal spectroscopy of the world ocean tides from a finite element hydrodynamic model, J. Geophys. Res., 99(C12), 24777–24798, 1994. 1704

Martin, P. J., Smith, S. R., Posey, P. G., Dawson, G. M., and Riedlinger, S. H.: Use of the Oregon State University Tidal Inversion Software (OTIS) to generate improved tidal prediction in the East-Asian Seas, Stennis Space Center, MS, Mississippi, 39529-5004, 2009.

Matsumoto, K., Takanezawa, T., and Ooe, M.: Ocean tide models developed by assimilating TOPEX/Poseidon altimeter data into hydrodynamic model: a global model and a regional model around Japan, J. Oceanogr., 56, 567–581, 2000. 1705

Pugh, D. T.: Tides, Surges and Mean Sea-Level, John Wiley and Sons, New York, 472 pp., 1987. 1705

Ray, R. D.: A global ocean tide model from TOPEX/Poseidon alrimetry: GOT99.2, NASA Tech. Memo. 209478, Goddard Space Flight Center, Greenbelt, 58 pp., 1999. 1705

Ray, R. D.: GSFC TOPEX/Poseidon "no-tide" data, (rray@geodesy2.gsfc.nasa.gov), Goddard Space Flight Center, Greenbelt, 2002.

Tsimplis, M. N., Proctor, R., and Flather, R. A.: A two-dimensional tidal model for the Mediterranean Sea, J. Geophys. Res., 100(C8), 16223–16239, 1995. 1709, 1712, 1713, 1714, 1723

OSD

7, 1703–1737, 2010

Table 1. Time period, number of records and sources of tide-gauge stations

Station number	Tide-gauge station	Time period from	to	Number of records	Source
1	Ajaccio	25-09-2000	1-11-2009	60 406	SONEL
2	Alexandroupolis	10-02-1986	10-12-1987	9876	HNHS
3	Algeciras	1-01-1998	27-09-2002	40 234	IEO
4	Almeria	1-09-2008	13-03-2010	10 387	PdE
5	Ancona	2-01-2006	15-10-2009	32 696	ISPRA
6	Antalya	1-01-1999	25-12-2005	58 472	ESEAS
7	Bakar	2-10-2004	27-05-2006	14 442	ESEAS
8	Barcelona2	1-09-2008	13-03-2010	9796	PdE
9	Bari	2-01-2006	15-10-2009	32 443	ISPRA
10	Cagliari	2-01-2006	15-10-2009	32 632	ISPRA
11	Carloforte	2-01-2006	15-10-2009	32 601	ISPRA
12	Catania	2-01-2006	15-10-2009	32 468	ISPRA
13	Ceuta	1-01-1995	31-12-2006	104 019	IEO
14	Chios	25-02-1986	5-11-1987	10 884	HNHS
15	Civitavecchia	2-01-2006	15-10-2009	32 621	ISPRA
16	Crotone	2-01-2006	15-10-2009	32 197	ISPRA
17	Dubrovnik	1-01-1999	30-12-2005	61 344	ESEAS
18	Gandia	1-09-2008	13-03-2010	9593	PdE
19	Genova	2-01-2006	15-10-2009	32 490	ISPRA
20	Gibraltar	17-02-2009	7-03-2010	9124	POL
21	Hadera	6-02-2003	30-04-2007	28 914	UHSLC
22	Imperia	2-01-2006	15-10-2009	32 424	ISPRA
23	Lampedusa	2-01-2006	15-10-2009	31 597	ISPRA
24	La Spezia	14-03-2006	15-10-2009	32 540	ISPRA
25	Leros	1-01-1986	29-11-1987	14 088	HNHS
26	Livorno	2-01-2006	15-10-2009	32 643	ISPRA
27	Mallorca	22-05-2003	31-05-2005	17 394	IEO
28	Marseille	1-01-2000	27-11-2009	84 497	SONEL
29	Melilla	28-02-2008	13-03-2010	13 185	PdE
30	Messina	2-01-2006	15-10-2009	32 669	ISPRA
31	Monaco	28-01-2000	7-12-2009	85 917	SONEL
32	Motril2	26-03-2008	14-03-2010	13 247	PdE
33	Napoli	5-01-2006	15-10-2009	32 133	ISPRA
34	Nice	1-01-2000	26-11-2009	80 045	SONEL
35	Ortona	2-01-2006	15-10-2009	32 714	ISPRA
36	Otranto	2-01-2006	15-10-2009	32 348	ISPRA
37	Palermo	2-01-2006	15-10-2009	32 488	ISPRA
38	Palinuro	2-01-2006	15-10-2009	32 628	ISPRA
39	Porto Empedocle	4-01-2006	15-10-2009	32 497	ISPRA
40	Pireas	8-01-1986	27-12-1987	14 712	HNHS
41	Porto Torres	2-01-2006	15-10-2009	32 357	ISPRA
42	Porto Vendres	26-10-2007	26-11-2009	18 188	SONEL
43	Rafina	9-01-1986	31-12-1987	9372	HNHS
44	Ravenna	2-01-2006	15-10-2009	32 381	ISPRA
45	Reggio Calabria	2-01-2006	15-10-2009	32 605	ISPRA
46	Rovinj	1-01-1999	30-12-2005	61 344	ESEAS
47	Sagunto	2-09-2008	13-3-2010	10 709	PdE
48	Salerno	2-01-2006	15-10-2009	32 638	ISPRA
49	Sete	1-01-2000	1-11-2009	69 095	SONEL
50	Souda	1-01-1986	31-12-1987	14 952	HNHS
51	Split	1-01-1999	30-12-2005	61 344	ESEAS
52	Taranto	2-01-2006	15-10-2009	32 161	ISPRA
53	Tarifa	1-01-1994	31-12-2005	104 503	IEO
54	Thessaloniki	12-03-1986	5-12-1987	12 960	HNHS
55	Toulon	1-01-2000	26-11-2009	82 743	SONEL
56	Trieste	2-01-2006	12-9-2008	22 747	ISPRA
57	Venezia	2-01-2006	15-10-2009	32 630	ISPRA
58	Vieste	2-01-2006	15-10-2009	32 693	ISPRA
59	Zadar	2-01-1991	30-12-2005	103 045	ESEAS

OSD
7, 1703–1737, 2010

A new assimilation tidal model for the Mediterranean Sea

D. N. Arabelos et al.

Table 2. Correlation coefficients larger than 0.01 between the constituents of Table 1. The numbers in parenthesis correspond to the stations of Table 1.

	Z_0	MF	MM	Q1	O1	K1	MU2	N2	M2	S2	MK3	SK3	S4
Z_0	–	.033	.052	–	–	.019	.011	–	–	–	–	.017	–
	–	(40)	(2)	–	–	(18)	(4)	–	–	–	–	(18)	–
MF		.017	–	.017	.018	–	–	–	–	–	–	–	–
		(43)	–	(18)	(18)	–	–	–	–	–	–	–	–
MM			.023	–	.017	.013	–	–	–	–	–	–	–
			(32)	–	(8)	(47)	–	–	–	–	–	–	–
Q1				–	.038	.036	–	.015	–	–	–	–	–
				–	(2)	(18)	–	(18)	–	–	–	–	–
O1					–	.023	–	.015	015	–	–	–	–
					–	(40)	–	(8)	(18)	–	–	–	–
K1						–	.012	–	–	.014	–	–	–
							(29)	–	–	(18)	–	–	–
MU2							–	.068	.030	.013	–	–	–
							–	(2)	(8)	(4)	–	–	–
N2								–	.037	.019	–	–	–
								–	(2)	(32)	–	–	–
M2									–	.025	.015	–	–
									–	(8)	(18)	–	–
S2										–	–	.019	.017
												(18)	(18)
MK3											–	.027	–
											–	(8)	–
SK3												–	–
													–
S4													–

Table 3. Vectorial differences between modeled and observed amplitudes and phases according to formula 17 for the control set of 54 tide-gauges of Sect. 5. Unit is cm.

	Site	M2	S2	K 1	O1	N2	P1	K2	Q1
1	Ajaccio	0.52	0.34	0.52	0.06	0.12	0.19	0.16	0.10
2	Alexandroupolis	3.91	2.08	0.79	0.23	0.51	0.51	0.50	0.16
4	Almeria	0.51	0.10	0.31	0.23	0.20	0.25	0.18	0.23
5	Ancona	1.68	0.78	2.09	1.84	0.14	1.07	0.45	0.54
6	Antalya	2.71	1.89	0.58	0.33	0.53	0.31	0.70	0.05
7	Bakar	0.33	1.71	5.32	2.73	0.56	4.29	0.16	0.85
8	Barcelona2	0.15	0.58	0.40	0.16	0.20	0.22	0.18	0.08
9	Bari	0.26	0.26	0.69	0.28	0.49	0.33	0.59	0.05
10	Cagliari	1.01	0.57	0.59	0.19	0.18	0.08	0.25	0.15
11	Carloforte	0.95	0.56	0.43	0.18	0.27	0.17	0.23	0.12
12	Catania	0.21	0.49	0.39	0.19	0.12	0.11	0.25	0.09
14	Chios	1.11	0.64	0.46	0.07	0.24	0.39	0.07	0.05
15	Civitavecchia	2.22	0.44	0.96	0.22	0.60	0.19	0.23	0.13
16	Crotone	0.30	0.36	0.15	0.01	0.05	0.14	0.19	0.02
17	Dubrovnik	0.71	0.65	0.10	0.21	0.44	0.26	0.63	0.07
18	Gandia	0.23	0.62	0.38	0.20	0.22	0.24	0.18	0.24
19	Genova	0.51	0.43	0.65	0.06	0.13	0.15	0.12	0.15
20	Gibraltar	1.67	0.59	0.58	0.65	0.31	0.30	0.48	0.13
21	Hadera	0.77	0.45	0.24	0.16	0.39	0.16	0.39	0.07
22	Imperia	1.28	0.51	0.51	0.02	0.11	0.23	0.07	0.14
23	Lampedusa	0.64	0.66	0.24	0.31	0.43	0.29	0.30	0.06
24	La Spezia	0.45	0.44	0.58	0.11	0.22	0.14	0.21	0.15
25	Leros	0.97	0.29	0.34	0.13	0.16	0.29	0.14	0.07
26	Livorno	0.80	0.50	0.47	0.27	0.28	0.11	0.22	0.15
27	Mallorca	0.21	0.29	0.46	0.11	0.15	0.21	0.12	0.24
28	Marseille	0.90	0.18	0.65	0.21	0.12	0.24	0.10	0.05
29	Melilla	2.58	1.42	1.65	1.51	0.75	0.72	0.59	0.20
30	Messina	6.89	3.10	2.55	0.66	1.35	0.78	0.92	0.47
32	Motril2	0.55	0.48	0.14	0.28	0.22	0.29	0.38	0.20
33	Napoli	0.27	0.27	0.65	0.20	0.08	0.09	0.18	0.17
34	Nice	0.47	0.34	0.39	0.04	0.09	0.19	0.13	0.06
35	Ortona	0.78	0.30	2.23	0.71	0.61	0.24	0.81	0.24
36	Otranto	0.27	0.48	0.38	0.20	0.18	0.24	0.36	0.06
37	Palermo	0.91	0.46	0.90	0.05	0.26	0.16	0.13	0.17
38	Palinuro	0.54	0.27	0.67	0.24	0.13	0.01	0.27	0.16
39	Porto Empedocle	0.86	0.89	0.04	0.04	0.42	0.20	0.28	0.06
40	Pireas	1.08	0.69	0.39	0.12	0.15	0.26	0.18	0.09
41	Porto Torres	3.85	1.42	1.40	0.41	0.72	0.55	0.31	0.23
42	Porto Vendres	0.16	0.38	0.36	0.06	0.19	0.16	0.19	0.08
43	Rafina	1.25	0.56	0.48	0.15	0.17	0.32	0.13	0.20
44	Ravenna	0.45	4.82	2.22	2.73	0.66	2.07	0.59	0.78
46	Rovinj	1.72	1.82	2.47	2.60	0.77	2.09	0.46	0.69
47	Sagunto	1.74	0.06	4.25	2.47	0.44	1.29	0.07	0.28
48	Salerno	0.72	0.33	0.55	0.22	0.15	0.01	0.33	0.13
49	Sete	0.23	0.41	0.60	0.09	0.22	0.17	0.20	0.02
50	Souda	0.52	0.39	0.34	0.21	0.17	0.28	0.10	0.03
51	Split	6.54	5.13	8.08	2.56	1.18	2.59	1.44	0.47
52	Taranto	0.10	0.54	0.09	0.07	0.12	0.11	0.19	0.04
54	Thessaloniki	4.59	2.22	0.97	0.22	0.30	0.63	0.48	0.08
55	Toulon	4.64	2.32	3.35	1.87	1.43	1.09	0.72	0.28
56	Trieste	5.53	2.36	3.29	3.04	1.86	2.51	1.39	0.67
57	Venezia	3.63	2.91	2.30	3.05	1.43	2.25	1.27	0.76
58	Vieste	1.05	0.65	1.18	0.49	0.52	0.56	0.54	0.07
59	Zadar	4.70	2.81	11.95	3.65	0.96	3.82	0.80	0.47

OSD

7, 1703–1737, 2010

A new assimilation tidal model for the Mediterranean Sea

D. N. Arabelos et al.

Table 4. Statistics of the differences (modeled–observed) at all sites of each tidal constituent of Table 3.

	Amplitude (cm)		Phase (°)	
	Mean difference	Standard deviation	Mean difference	Standard deviation
M2	−0.272	1.659	−0.059	0.312
S2	−0.063	1.163	0.001	0.310
K1	−0.207	2.216	−0.060	0.939
O1	−0.342	1.114	0.035	0.246
N2	−0.117	0.460	−0.002	0.572
P1	−0.266	0.987	0.511	2.048
K2	0.036	0.387	−0.037	0.920
Q1	−0.073	0.154	−0.245	1.253

OSD
7, 1703–1737, 2010

Table 5. Vectorial differences between modeled and observed amplitudes and phases according to Eq. (17) for the control set of 20 tide-gauges taken from Tsimplis et al. (1995). Unit is cm.

	Site	M2	S2	K1	O1
60	Alicante	0.31	0.18	0.84	0.40
61	Skikda	0.41	0.29	1.91	0.21
62	Gabes	3.52	4.52	0.40	1.00
63	Sfax	8.93	6.14	0.86	0.61
64	Zarzis	1.83	5.97	0.62	0.30
65	Panteleria	1.04	0.88	0.59	–
66	Tripoli	1.69	1.80	0.59	0.48
67	Malta	1.54	0.99	0.89	0.30
68	Bar	0.58	0.69	0.17	0.22
69	Lefkas	1.61	1.25	0.34	0.10
70	Katakolo	0.85	0.84	0.20	0.11
71	Kalamata	1.28	0.85	0.22	0.01
72	Tobruch	1.28	0.87	0.22	0.23
73	Iraklion	0.65	0.62	0.33	0.27
74	Portobardia	1.09	0.62	0.37	0.40
75	Rodos	1.49	1.12	0.21	0.25
76	Alexandria	0.62	0.84	0.17	0.12
77	Portsaid	0.22	0.52	0.24	0.12
78	Kyrenia	0.50	0.67	0.20	0.18
79	Famagusta	0.22	1.08	0.71	0.20

OSD
7, 1703–1737, 2010

A new assimilation tidal model for the Mediterranean Sea

D. N. Arabelos et al.

Table 6. Statistics of the differences at all sites of each tidal constituent of Table 5.

	Amplitude (cm)		Phase (°)	
	Mean difference	Standard deviation	Mean difference	Standard deviation
M2	−0.120	1.456	−0.050	0.267
S2	−0.325	1.875	−0.058	0.232
K1	0.120	0.520	−0.613	1.914
O1	−0.375	2.210	−0.012	0.299

Discussion Paper | Discussion Paper | Discussion Paper | Discussion Paper |

OSD

7, 1703–1737, 2010

A new assimilation tidal model for the Mediterranean Sea

D. N. Arabelos et al.

Table 7. Statistics of the crossover differences of raw JASON-1 data before and after the tidal correction using global and regional models. Last column shows the improvement per cent of the standard deviation. Unit is m.

Crossover differences	Number of crossovers	Mean value	Standard deviation	Minimum difference	Maximum difference	Percentual improvement
JASON1 (raw data)	124 244	−0.0086	0.1497	−0.70	0.63	–
JASON1-MED2004	124 244	−0.0086	0.1251	−0.66	0.61	16.43%
JASON1-MED2008	124 244	−0.0084	0.1233	−0.68	0.60	17.64%
JASON1-GOT00.2	124 244	−0.0079	0.1244	−0.68	0.59	16.90%
JASON1-NAO99b	124 244	−0.0086	0.1251	−0.69	0.59	16.43%
JASON1-MEDI10	124 244	−0.0084	0.1234	−0.69	0.60	17.57%

Table 8. Statistics of the differences of the tidal heights computed from the models MEDI10, MED2008, GOT00.2 and NAO99b at 20 different time moments on a grid covering the Mediterranean Sea. Unit is m.

	Number of points	Mean value	Standard deviation	Minimum difference	Maximum difference
MED2008−MEDI10	80 720	−0.000283	0.008473	−0.2044	0.1761
GOT00.2−MEDI10	73 840	0.003356	0.015153	−0.2791	0.2910
NAO99b−MEDI10	82 480	0.000470	0.021210	−0.5261	0.3622

OSD
7, 1703–1737, 2010

A new assimilation tidal model for the Mediterranean Sea

D. N. Arabelos et al.

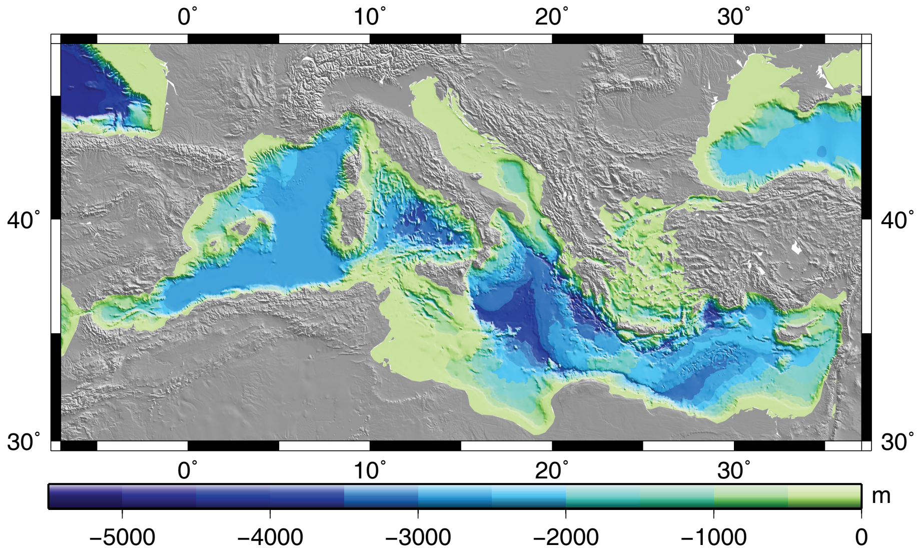

Fig. 1. Bathymetry in the Mediterranean Sea.

OSD
7, 1703–1737, 2010

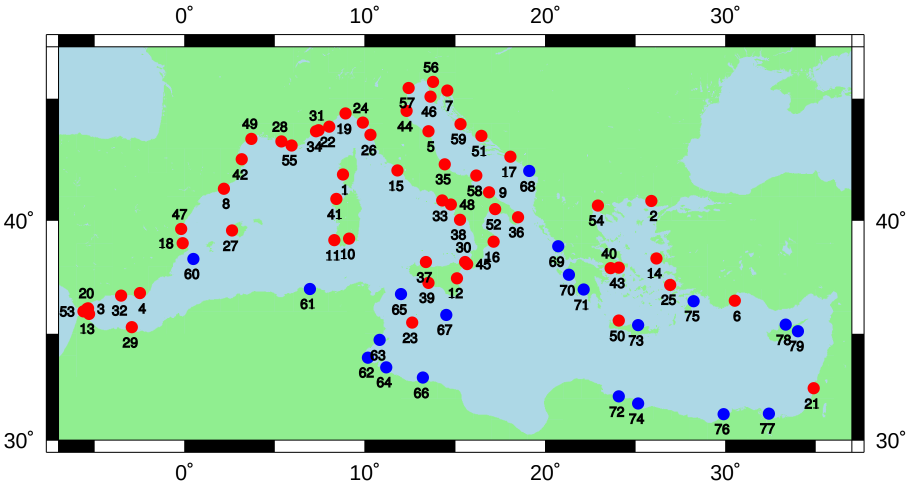

Fig. 2. Distribution of tide-gauge stations along the coasts of the Mediterranean Sea. In red the stations included in Table 1 are shown. For the stations in blue tidal parameters for M2, S2, K1, and O1 were used from Tsimplis et al. (1995).

OSD
7, 1703–1737, 2010

A new assimilation tidal model for the Mediterranean Sea

D. N. Arabelos et al.

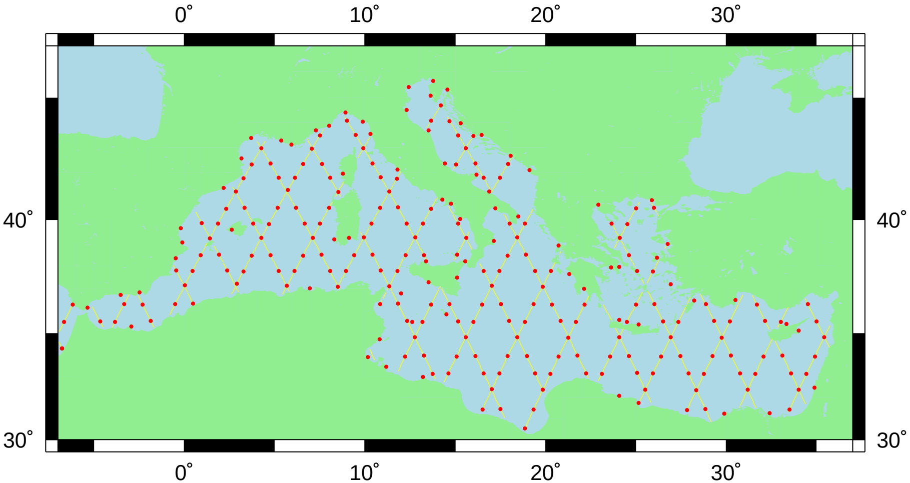

Fig. 3. Representers and data sites used for the computation of MEDI10.

OSD
7, 1703–1737, 2010

A new assimilation tidal model for the Mediterranean Sea

D. N. Arabelos et al.

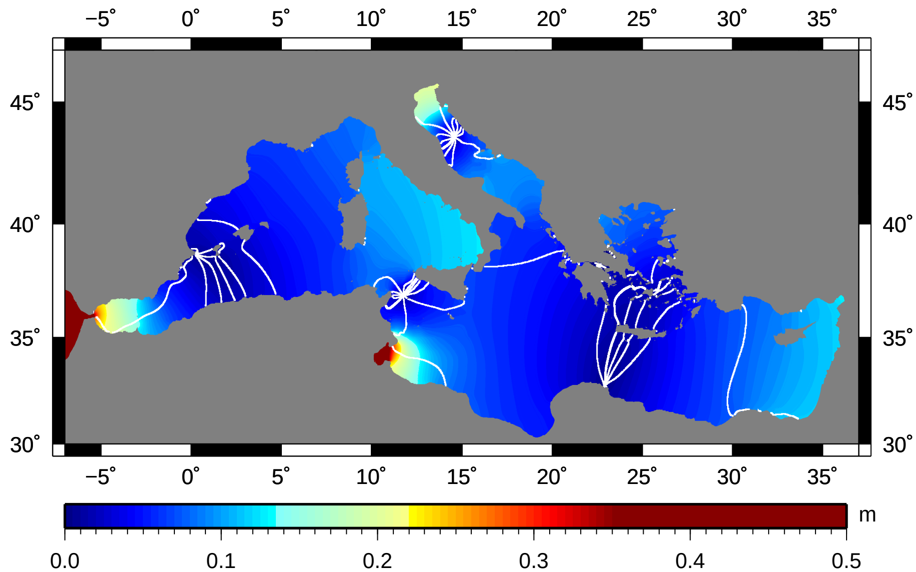

Fig. 4. Amplitude and phase of the M2 constituent.

OSD

7, 1703–1737, 2010

A new assimilation tidal model for the Mediterranean Sea

D. N. Arabelos et al.

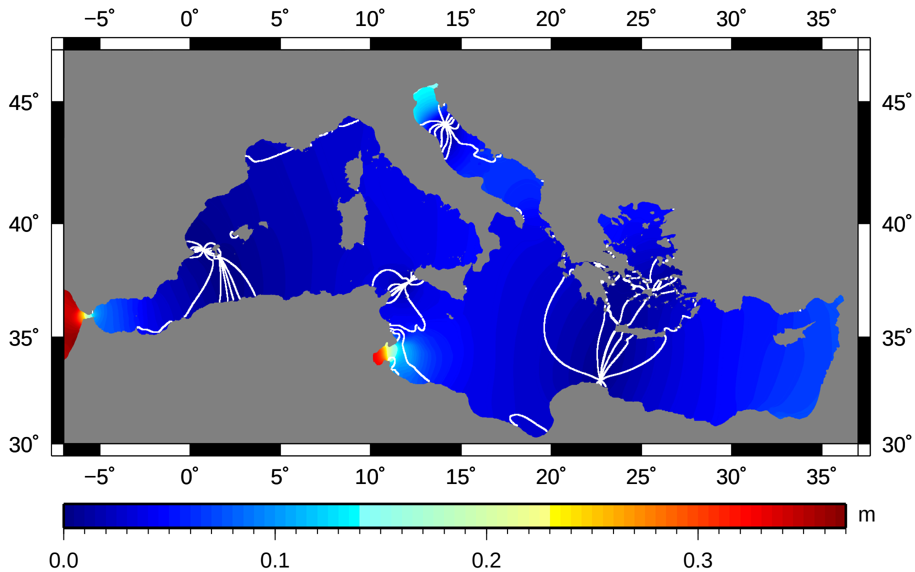

Fig. 5. Amplitude and phase of the S2 constituent.

OSD
7, 1703–1737, 2010

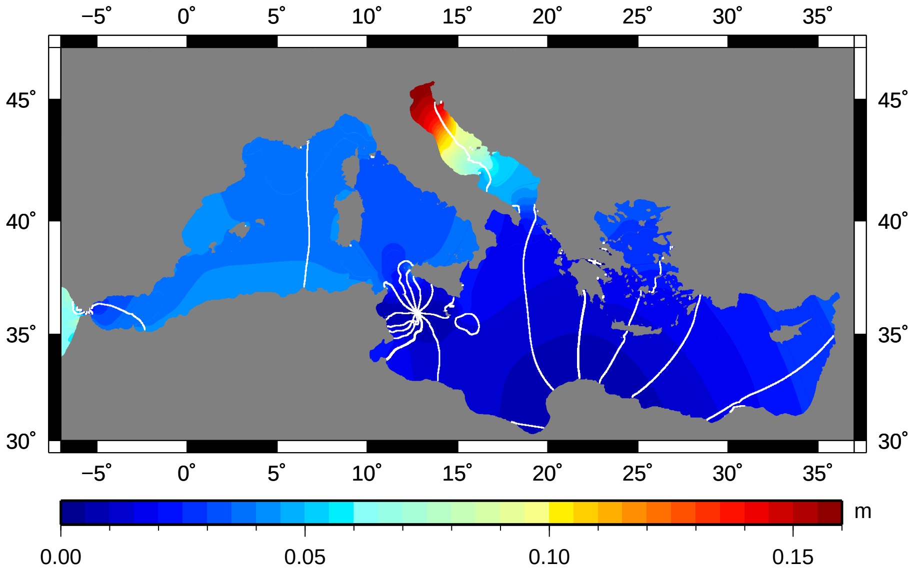

Fig. 6. Amplitude and phase of the K1 constituent.

OSD
7, 1703–1737, 2010

A new assimilation tidal model for the Mediterranean Sea

D. N. Arabelos et al.

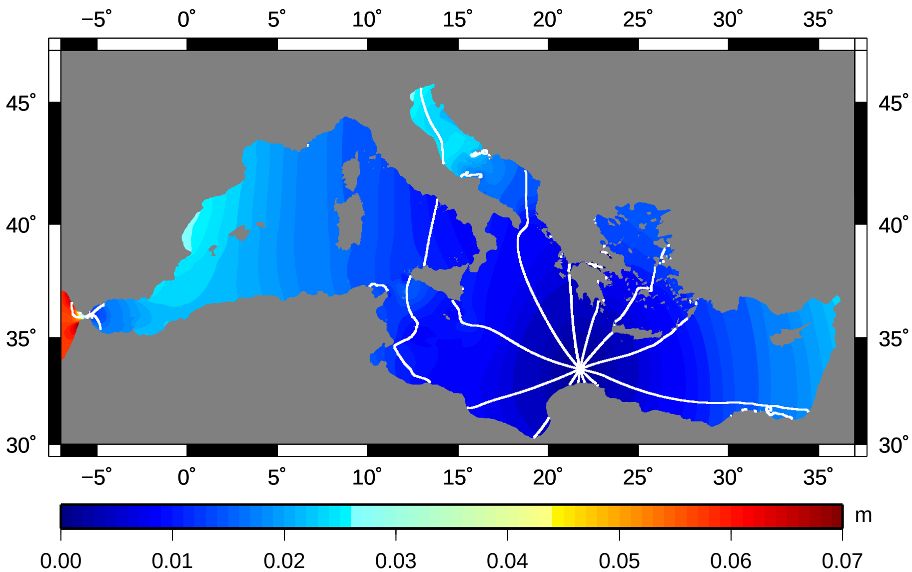

Fig. 7. Amplitude and phase of the O1 constituent.

OSD

7, 1703–1737, 2010

A new assimilation tidal model for the Mediterranean Sea

D. N. Arabelos et al.

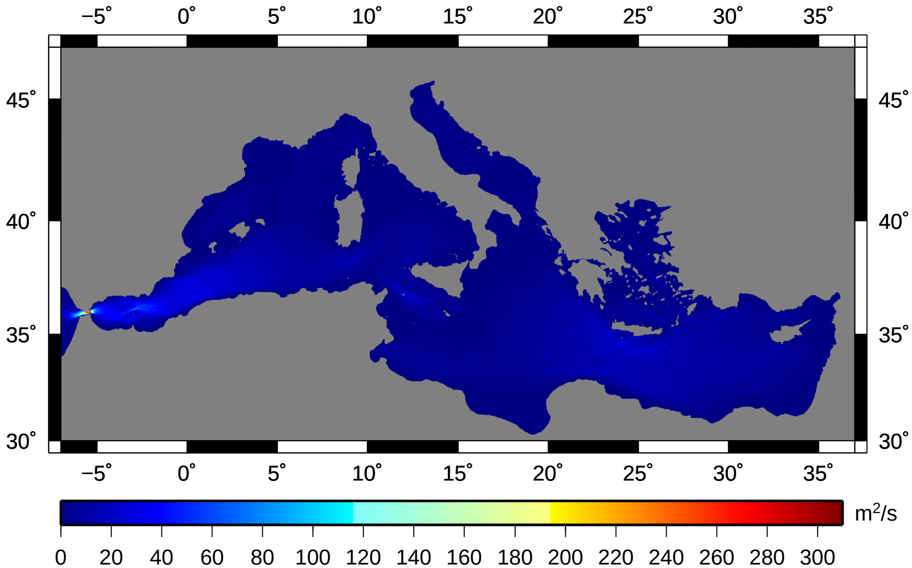

Fig. 8. Amplitude of the W-E transports of M2 constituent.

OSD
7, 1703–1737, 2010

A new assimilation tidal model for the Mediterranean Sea

D. N. Arabelos et al.

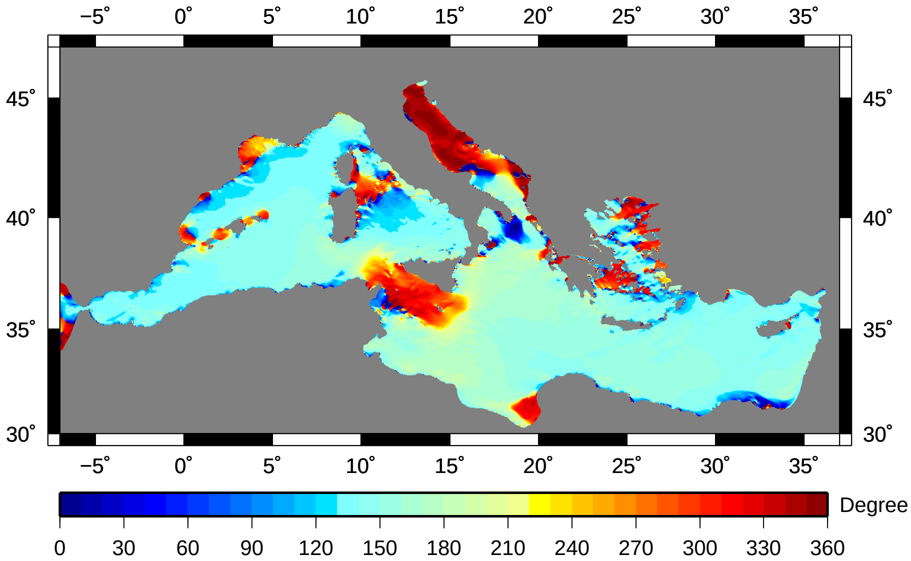

Fig. 9. Phase of the W-E transports of M2 constituent.

OSD
7, 1703–1737, 2010

A new assimilation tidal model for the Mediterranean Sea

D. N. Arabelos et al.

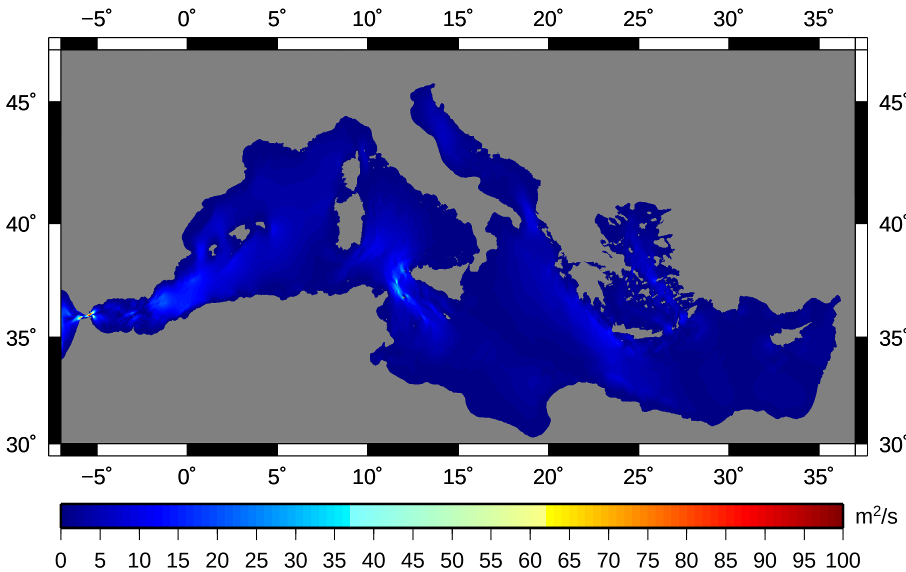

Fig. 10. Amplitude of the S-N transports of M2 constituent.

OSD

7, 1703–1737, 2010

A new assimilation tidal model for the Mediterranean Sea

D. N. Arabelos et al.

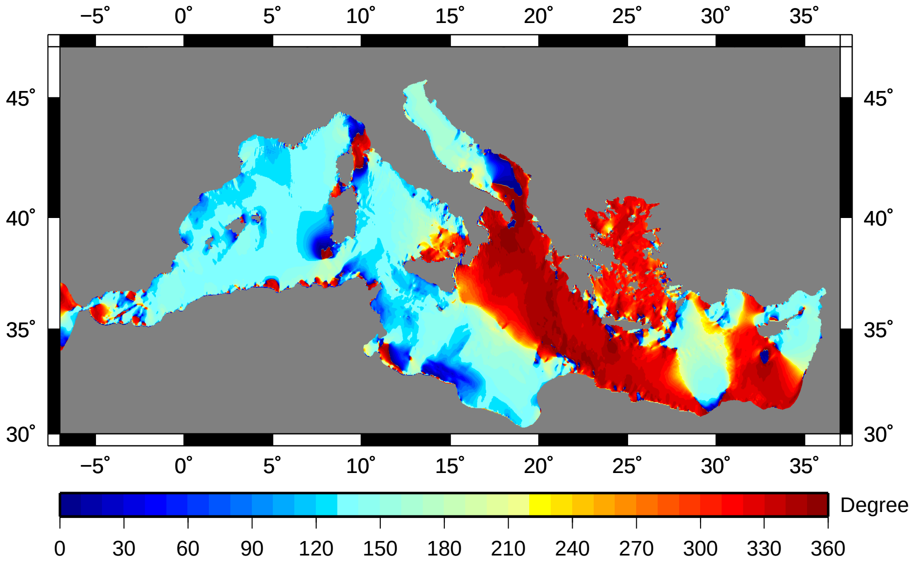

Fig. 11. Phase of the S-N transports of M2 constituent.

OSD

7, 1703–1737, 2010

A new assimilation tidal model for the Mediterranean Sea

D. N. Arabelos et al.